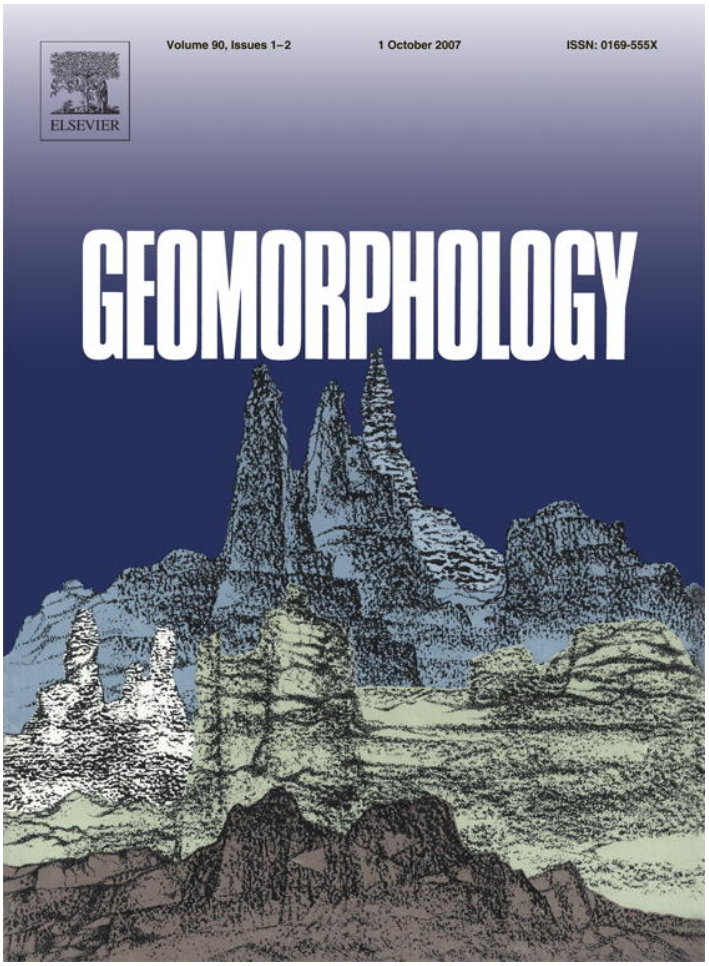

Available online at www.sciencedirect.com
ScienceDirect
Geomorphology 90 (2007) 23–35
GEOMORPHOLOGY
www.elsevier.com/locate/geomorph

Modelling landslide hazard, soil redistribution and sediment yield of landslides on the Ugandan footslopes of Mount Elgon

L. Claessens [a,*], A. Knapen [b], M.G. Kitutu [c], J. Poesen [b], J.A. Deckers [d]

[a] *International Potato Center (CIP), Sub-Saharan Africa Regional Office, Natural Resource Management Division, PO Box 25171, Nairobi 00603, Kenya*
[b] *Physical and Regional Geography Research Group, K.U. Leuven, Celestijnenlaan 200 E, BE-3001 Heverlee, Belgium*
[c] *National Environment Management Authority, P.O. Box 22255, Kampala, Uganda*
[d] *Division of Soil and Water Management, K.U. Leuven, Celestijnenlaan 200 E, BE-3001 Heverlee, Belgium*

Received 14 August 2006; received in revised form 9 January 2007; accepted 10 January 2007
Available online 17 January 2007

Abstract

In this study, the LAPSUS-LS landslide model, together with a digital terrain analysis of topographic attributes, is used as a spatially explicit tool to simulate recent shallow landslides in Manjiya County on the Ugandan slopes of Mount Elgon. Manjiya County is a densely populated mountainous area where landslides have been reported since the beginning of the twentieth century. To better understand the causal factors of landsliding, 81 recent landslides have been mapped and investigated. Through statistical analysis it was shown that steep concave slopes, high rainfall, soil properties and layering as well as human interference were the main factors responsible for landslides in the study area. LAPSUS-LS is used to construct a landslide hazard map, and to confirm or reject the main factors for landsliding in the area. The model is specifically designed for the analysis of shallow landslide hazard by combining a steady state hydrologic model with a deterministic infinite slope stability model. In addition, soil redistribution algorithms can be applied, whereby erosion and sedimentation by landsliding can be visualized and quantified by applying a threshold critical rainfall scenario. The model is tested in the Manjiya study area for its ability to delineate zones that are prone to shallow landsliding in general and to group the recent landslides into a specific landslide hazard category. The digital terrain analysis confirms most of the causal topographic factors for shallow landsliding in the study area. In general, shallow landslides occur at a relatively large distance from the water divide, on the transition between steep concave and more gentle convex slope positions, which points to concentration of (sub)surface flow as the main hydrological triggering mechanism. In addition, LAPSUS-LS is capable to group the recent shallow landslides in a specific landslide hazard class (critical rainfall values of 0.03–0.05 m day^{-1}). By constructing a landslide hazard map and simulating future landslide scenarios with the model, slopes in Manjiya County can be identified as inherently unstable and volumes of soil redistribution can yield four times higher than currently observed. More than half of this quantity can end up in the stream network, possibly damming rivers and causing major damage to infrastructure or siltation and pollution of streams. The combination of a high population density, land shortage and a high vulnerability to landslides will likely continue to create a major sustainability problem.

Keywords: LAPSUS-LS; Landslide hazard mapping; Uganda; Manjiya; Shallow landslides

* Corresponding author. Tel.: +254 20 422 3612; fax: +254 20 422 3001.
E-mail address: l.claessens@cgiar.org (L. Claessens).

0169-555X/$ - see front matter © 2007 Elsevier B.V. All rights reserved.
doi:10.1016/j.geomorph.2007.01.007

1. Introduction

Although landsliding has been recognized as a widespread phenomenon in the East African highlands, having a great social, economic and geomorphological impact, relatively little research and documentation can be found in the international literature (Ngecu and Mathu, 1999; Knapen et al., 2006). High annual rainfall, steep slopes, deforestation, high weathering rates and slope material with a low shear strength or high clay content are considered the preparatory causal factors for mass movements. In addition, increasing population pressure, with slope disturbance, inconsiderate irrigation and deforestation as consequences and such triggering factors as earthquakes and extreme rainfall events turn the East African highlands into a inherently susceptible region (Glade and Crozier, 2004).

Previous, qualitative studies on landsliding in East Africa have been conducted in Kenya (Davies, 1996; Ngecu and Ichangi, 1998; Westerberg and Christiansson, 1998; Ngecu and Mathu, 1999), Rwanda (Moeyersons, 1989, 2003), Tanzania (Christiansson and Westerberg, 1999), Ethiopia (Nyssen et al., 2002) and Uganda (Muwanga et al., 2001). Nevertheless, a complete understanding of local causal factors or a more landscape-wide and quantitative approach on causes and consequences of landsliding is yet lacking.

In Uganda, landslides are common in the mountainous areas of the districts Sironko, Kapchorwa, Mbale, Kabale, Rukungiri, Mbarara, Kasese, Bushenyi, Bundibugyo and Kanungu (Fig. 1)) but so far almost no systematic scientific research has been conducted on this topic (Muwanga et al., 2001; Knapen et al., 2006). Manjiya County, within the Mbale district and situated on the southwestern footslopes of the Mount Elgon volcano, is the most sensitive area for landslides in Uganda. Mass movements associated with intense rainstorms are reported to have occurred periodically in Manjiya since the early 20th century but the increase in fatalities and losses as a consequence of the enormous population growth draws attention to the phenomenon nowadays (Knapen et al., 2006).

Breugelmans (2003), Knapen (2003), and Knapen et al. (2006) conducted a first study on the characteristics and causal factors of landslides in Manjiya. They mapped and investigated 98 recent landslides that together displaced about 11 million m^3 of slope material. By statistically comparing topographical characteristics

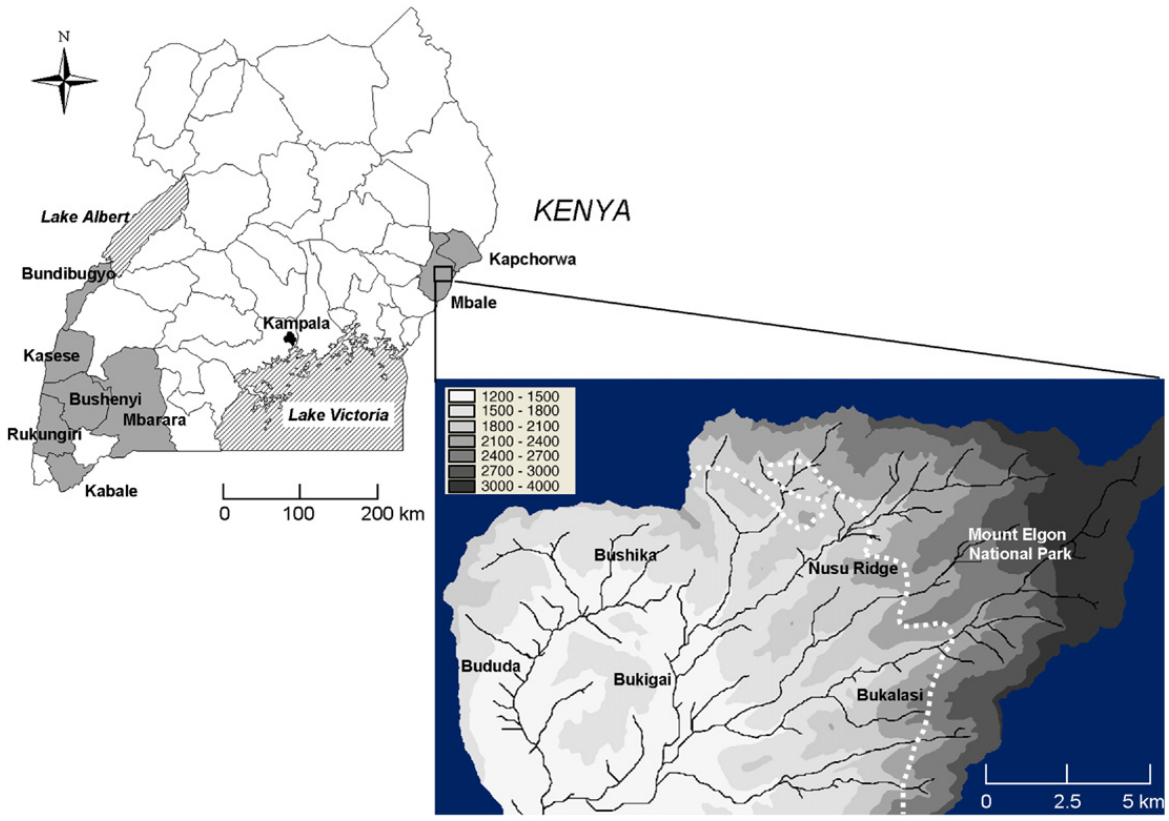

Fig. 1. Location of the study area within the Mbale district and other districts in Uganda vulnerable to landslide activity (shaded in grey). Grey tones in the study area (down right) reflect altitude zones based on the DEM.

from landslide sites with those from the whole study area, it was shown that landslides occur predominantly on steep concave slopes that are oriented to the main rainfall direction (northeast) and at a relatively large distance from the water divide. Furthermore, the Manjiya area was divided into different zones based on landslide type (rotational or translational) and frequency of occurrence.

Elaborating on these results, this paper investigates the suitability of the LAPSUS-LS landslide model (Claessens et al., 2005) as a spatially explicit tool to delineate zones which are prone to landsliding in general and to group the observed landslides in a specific landslide type and hazard category. Furthermore, an attempt is made to revisit the main causal factors for landsliding in Manjiya and to use the model to simulate possible landslide scenarios with resulting sediment yields and geomorphic impacts for the region.

2. Study area

Manjiya County is located on the southwestern footslopes of the extinct Mount Elgon shield volcano, in the Mbale district on the border of Uganda and Kenya (Fig. 1).[1] The volcano stands at 4322 m a.s.l. and is of Pliocene age. The 275 km^2 study area of Manjiya County is bounded by latitude 2° 49′–2° 55′N and longitude 34° 15′–34° 34′E. Altitude ranges from 1300 to 2850 m a.s.l. Because of this high altitude, precipitation values are high with an annual average of 1800 mm. Two distinct wet seasons can be distinguished, separated by a pronounced dry period from December to February and by a period of dispersed, less intense rains from July to early August. The mean annual air temperature is about 23 °C (National Environment Management Authority, 2001).

Volcanic rocks are restricted to the northern and eastern remote corner of the study area and to some isolated dikes and plugs. The strongly weathered granites of the Basement Complex, which cover a large part of the East African Plain, dominate the geology of Manjiya (Davies, 1957). In the central part of the study area, Bukigai, a magmatic carbonatite intrusion has caused fenitization in the surrounding granites (Reedman, 1973). Fenitization implies the chemical alteration of the country rock by migrating fluids with shattering and shearing of the country rock as a consequence, possibly leading to an increased sensitivity to slope instability (Knapen et al., 2006). The geomorphology of the study area is dominated by this carbonatite hill that has caused the doming of the country rock and created a broad concentric valley around it. The majority of the rivers in Manjiya collect into a single river in this valley that finally drains in the Lake Kyoga swamps in the southeast. West of the concentric valley, gentle concave slopes can be found that contrast with the steeper rectilinear and sharply dissected slopes in the east (Knapen et al., 2006).

The dominant soil types in the study area, according to the WRB classification (Deckers et al., 1998), are Acrisols, Ferralsols, Nitisols and Luvisols. On the western slopes, deep Nitisols occur whereas on the steep slopes in the east, shallow soils dominate. Depending on the position on the slopes, Ferralsols and Acrisols can be found on the central carbonatite hill (Breugelmans, 2003). Soil scientists are currently revisiting the area to make a more detailed soil classification (Kitutu, personal communication).

Average population density amounts 952 persons km^{-2} for Manjiya County (Uganda Bureau of Statistics, 2004), with >1300 persons km^{-2} in the densely populated western part. Due to land scarcity land parcels are small and even slopes steeper than 80% are cultivated (Knapen et al., 2006). The main crops grown in the subsistence agricultural system are banana, yam, cassava, sweet potato and maize. Nowadays, forest constitutes 45% of Manjiya County, whereas before the large-scale deforestation starting in the 1930s, the forest was more extensive and most slopes east of Bukigai were under forest (Hamilton, 1984).

3. Materials and methods

3.1. Landslide mapping

During August and September 2002, an intensive field survey was undertaken to determine the spatial distribution and field characteristics of landslides in Manjiya. Details of this survey can be found in Breugelmans (2003), Knapen (2003), and Knapen et al. (2006). The surveys were restricted to the part of the study area outside Mount Elgon National Park (Fig. 1). Because of the fast regeneration of vegetation after slope failures, older landslide scarps are hard to distinguish and only those that were still clearly visible during the field survey were mapped. The geographic positions and dimensions of the landslides were obtained with a GPS device and measuring tapes respectively.

[1] In December 2005 new district borders were created. The Mbale district was divided into the Mbale and Manafwa districts. Manjiya County was located in the Manafwa district. In August 2006, the Manafwa district is again split up, placing Manjiya in the Bududa district.

3.2. LAPSUS-LS landslide model

The LAPSUS modelling framework was originally developed to study the long-term effects of geomorphic processes at the landscape scale (Schoorl et al., 2000). To include the impact of soil redistribution by shallow landslides, the LAPSUS-LS component was embedded in the model. The overall aim of LAPSUS-LS is to assess the impact of landsliding on landscape evolution and to identify possible feedbacks with other geomorphic processes; it is not intended to simulate detailed changes in hillslope geomorphology caused by individual failures. Despite its assumptions and limitations, this approach has been demonstrated to retain the essence of the physical control of topography and soil properties on landsliding and remains parametrically simple for ease of calibration and application (Claessens et al., 2005, in press).

LAPSUS-LS encompasses several modelling steps. First, relative landslide hazard distribution is calculated from spatially explicit topographical and soil physical data. Next, historical rainfall/landslide distribution datasets and magnitude/frequency scenarios can be used to calibrate and run the model for consecutive timesteps. Soil redistribution algorithms (erosion and sedimentation) are then applied to simulate and visualize feedbacks between mass movements or to analyze interactions with other hillslope processes. Although the model was originally not intended to quantify erosion or sedimentation, a spatially explicit sediment delivery algorithm was added to simulate scenarios of sediment yield from landslides at the catchment scale (Claessens et al., 2006a).

3.2.1. Relative hazard for shallow landsliding

For the analysis of shallow landslide hazard, a steady state hydrologic model is combined with a deterministic infinite slope stability model. This approach has been described previously by Montgomery and Dietrich (1994), and has performed well in a variety of applications (Montgomery et al., 2000; Pack et al., 2001; Claessens et al., 2006a,b). We calculate the minimum steady state critical rainfall predicted to cause slope failure, Q_{cr} [m day^{-1}], which can be written as:

$$Q_{cr} = T\sin\theta\left(\frac{b}{a}\right)\left(\frac{\rho_s}{\rho_w}\right)\left[1-\frac{(\sin\theta - C)}{(\cos\theta\tan\phi)}\right] \quad (1)$$

where T is saturated soil transmissivity [m^2 day^{-1}], θ local slope angle [°], a the upslope contributing drainage area [m^2], b the unit contour length (the grid resolution [m] is taken as the effective contour length as in Pack et al., 2001), ρ_s wet soil bulk density [g cm^{-3}], ρ_w the density of water [g cm^{-3}], ϕ the effective angle of internal friction of the soil [°] and C is the combined cohesion term [–], made dimensionless relative to the perpendicular soil thickness and defined as:

$$C = \frac{C_r + C_s}{h\rho_s g} \quad (2)$$

where C_r is root cohesion [N m^{-2}], C_s soil cohesion [N m^{-2}], h perpendicular soil thickness [m], and g the gravitational acceleration constant (9.81 m s^{-2}). The spatial distribution of critical rainfall values calculated according to Eq. (1) can be interpreted as an expression of the relative potential for shallow landslide initiation.

With the boundary conditions used in deriving Eq. (1) (refer to Claessens et al., in press), the conditions for upper and lower thresholds for elements that can possibly fail can be defined. Unconditionally stable areas are predicted to be stable, even when saturated and satisfy

$$\tan\theta \le \left(\frac{C}{\cos\theta}\right) + \left(1-\frac{\rho_w}{\rho_s}\right)\tan\phi \quad (3)$$

Unconditionally unstable elements are unstable even when dry and satisfy

$$\tan\theta > \tan\phi + \left(\frac{C}{\cos\theta}\right) \quad (4)$$

3.2.2. Failed landslide material redistribution

To determine landslide soil redistribution within a catchment, complex algorithms applicable to individual slope failures are inappropriate and therefore more simple, empirical formulae were developed (Claessens et al., in press). Following the initial failure, in the erosional phase, a depth of unstable soil material S [m] is eroded following the steepest descent direction and estimated as:

$$S = \frac{\rho_s\cos\theta(\tan\theta - \tan\alpha)\delta}{C_s} \quad (5)$$

with α [°] being minimum local slope for landslide erosion and δ [m^2] a dimensional correction factor. The point at which sedimentation begins is reached once the gradient falls below an area specific slope angle α. The elevation loss within the erosional phase is used as an index of momentum at the start of sedimentation. The number of downslope grid cells involved in the

sedimentation of landslide material, defined 'cell-distance' D [–], is calculated as:

$$D = \left(\frac{\Delta y \varphi}{b}\right) \quad (6)$$

where b is the grid resolution [m], Δy [m] the elevation difference between the head of the slide and the point at which sedimentation begins, and φ [–] an empirically derived 'runout fraction' (Vandre, 1985; Burton and Bathurst, 1998). To incorporate hillslope morphology into the spatial sedimentation pattern, the accumulated soil material is routed with multiple flow direction principles (Quinn et al., 1991): for down slope neighbours of the point where sedimentation starts, the sediment which is effectively delivered to grid cell i, is expressed as:

$$S_i = \left(\frac{B_{i-1}}{D_{i-1}}\right) f_i \quad (7)$$

The term B_{i-1}/D_{i-1} is the amount of sediment originating from erosion upslope (grid cell $i-1$), divided by the cell-distance (Eq. (6)), and deposited in grid cell i. f_i is the fraction allocated to each lower neighbour and determined by the multiple flow concept described by Quinn et al. (1991). The remaining sediment budget of grid cell i, which is not deposited but 'passed through' to grid cell $i+1$, can be written as:

$$B_i = B_{i-1}\left(1 - \frac{1}{D_{i-1}}\right) f_i \quad (8)$$

In each down-slope grid step, the cell-distance is lowered by one, and when $D<1$ all the remaining sediment is deposited.

3.2.3. Sediment yield and delivery ratio

A catchment's sediment yield produced by landsliding depends on whether the eroded material is deposited in, and transported by, the channel network. The percentage delivery or delivery ratio is dependent on the interaction between landslide soil redistribution patterns and streams capable to route and transport the sediment further towards the catchment outlet. Instead of estimating or extrapolating delivery ratios and sediment yields from site measurements or large field inventories, the sediment yield can be determined from the spatial pattern of soil redistribution modelled with LAPSUS-LS and the interaction with a topographically delineated stream network. Landslide soil material displacement is modelled using Eqs. (5)–(8).

Although different methods are available for determining a stream network, (e.g. O'Callaghan and Mark, 1984; Martin et al., 2002), for this application, the stream network is determined by specifying a minimum contributing area threshold. Flow direction was assigned according to the steepest descent, and flow accumulation was calculated as a measure of the drainage area in number of grid cells ('D8' algorithm; Fairfield and Leymarie, 1991). All grid cells draining more than a threshold drainage area are defined as part of the stream network and capable to transport landslide material to the catchment outlet. When a grid cell, which is part of the depositional pathway of a landslide, intersects with a grid cell from the transporting stream network, the remaining sediment budget of that grid cell, according to Eq. (8), is added to the total catchment sediment yield.

3.3. Digital terrain analysis and parameterisation LAPSUS-LS

Data requirements for the LAPSUS-LS model are good quality topographical information and the soil physical and hydrological parameters used in Eqs. (1)–(5) (Claessens et al., in press).

A Digital Elevation Model (DEM) was generated from the existing 1:50,000-scale topographic maps by digitizing the contours of the Manjiya County study area (Lands and Surveys Department Uganda, 1967). The vectorized contours with a 50-ft interval (~15 m) were interpolated to a 10×10 m resolution DEM with the 'Topo to Raster' function in ESRI ArcGIS 9.1. 'Topo to Raster' uses an interpolation method specifically designed for the creation of hydrologically correct DEMs. It is based on the ANUDEM program developed by Hutchinson (1989). Possible effects of choice of DEM resolution on the results of the LAPSUS-LS model are discussed in Claessens et al. (2005).

Topographic attributes computed from the DEM within the LAPSUS-LS model are the local (cell to cell) slope angle θ and the upslope contributing drainage area a, using both the steepest descent algorithm (Fairfield and Leymarie, 1991) and the algorithm of multiple downslope flow (Quinn et al., 1991). Contributing drainage area values are only calculated for the main stream catchment of the study area. The watershed boundary was delineated using ESRI ArcGIS 9.1 Spatial Analyst 'Basin' function. The surface area of the watershed is 13,360 ha.

Values for T, C, ρ_s and ϕ are stratified according to the three main soil associations in the study area (Central–West–East). These soil physical properties were measured for soils of the western and central parts of the study area (Soil Mechanics Laboratory, Makerere University, Kampala, Uganda; Kitutu, personal communication) and

estimated by comparing laboratory measurements and field observations (Breugelmans, 2003) with associated soil attributes found in the literature (Montgomery and Dietrich, 1994; Borga et al., 2002; Claessens et al., in press). Root strength of vegetation can provide significant apparent cohesion to the soil and is accounted for in the root cohesion term C_r in Eq. (2). Root cohesion is however hard to quantify, certainly spatially explicit at the catchment scale. In this application it is regarded as a lumped, constant parameter (with value zero) within the study area. In this way, the critical rainfall value (Eq. (1)) is reduced to a terrain intrinsic, relative landslide hazard index, not taking into account differences in root reinforcement attributed to different land cover. For an assessment of the sensitivity of the LAPSUS-LS model to variability of soil physical and topographic parameters, the reader is referred to Claessens et al. (2005).

The settings of the empirical parameters used in the soil redistribution algorithms (5)–(8) are based on field observations (Knapen, 2003) and literature (Vandre, 1985; Burton and Bathurst, 1998; Knapen, 2003; Knapen et al., 2006): the 'runout fraction' φ was set at 0.4 and the slope angle α at which sedimentation begins, was set at 10°. The threshold value of contributing area for stream development, to delineate streams capable to transport sediment to the catchment outlet was set at 5000 grid cells (50 ha), based on comparison of this DEM-derived stream network with the major streams indicated on the 1:50,000-scale topographic maps (Lands and Surveys Department Uganda, 1967).

For a digital terrain analysis of the topographic attributes determining landslide sites, maps with elevation, slope angle, aspect, profile and plan curvature for each pixel were deduced from the DEM in ESRI ArcGIS 9.1 using the algorithms of Zevenbergen and Thorne (1987). Elevation determines vertical climatic zones correlated with air temperature and rainfall. Slope angle and aspect can have an effect on soil moisture through their influence on potential evapotranspiration and exposure to wind and rainfall (Moore et al., 1993; Blocken et al., 2006; Claessens et al., 2006b). The profile curvature affects the acceleration and deceleration of flow and, therefore, influences erosion and sedimentation. A negative profile indicates that the surface is upwardly convex at that cell (typically on upper slopes where slope angle is increasing downhill). A positive profile indicates that the surface is upwardly concave at that cell (typically on lower slopes where slope is decreasing downhill). The plan (or contour) curvature influences convergence and divergence of flow. A positive plan indicates that the surface is upwardly convex at that cell (diverging flow, on ridges). A negative plan indicates that the surface is upwardly concave at that cell (converging flow, in valleys and channels) (Moore et al., 1991; Wilson and Gallant, 2000).

4. Results and discussion

4.1. Landslide mapping and previous findings

Eighty-one landslides, clearly distinguishable in the landscape, were mapped in the 2002 field survey and are contained within the spatial extent of the DEM (Knapen, 2003). Together they displaced ca. 10 million m^3 of slope material. The spatial distribution of the landslides in Manjiya is closely related with the factors influencing the stability and their spatial variation. By comparing the topographic variables of the slopes exhibiting landslides with those for the whole study area, topographic variables playing a significant part in slope instability can be discriminated. The initial study by Knapen et al. (2006) statistically showed (Chi-square and Cramer's *V*-tests) that the landslides in general are likely to occur on steep, concave slope segments oriented to the northeast, the direction of dominating rains, at a certain distance from the water divide. Furthermore, logistic regression revealed that rotational landslides dominate in deep soils, on the lower part of plan concave slopes, at a relatively large distance from the water divide. Translational landslides on the contrary, are more likely to occur in shallow soils on steep, rectilinear slopes. Based on the types, causes and distribution of landslides, Knapen et al. (2006) demarcated three main zones within the Manjiya study area (Fig. 1) as follows.

4.1.1. East — Nusu Ridge/Bukalasi

In the eastern part of the study area, many shallow translational landslides occur. Most soils have a distinct boundary between the soil and the underlying saprolite in common. This abrupt transition between the shallow soil and the bedrock serves as a shear plane during intense rainfall. Furthermore, recent deforestation plays a major role here. Manjiya County has been deforested since the 1930s (Hamilton, 1984) but spatial and temporal information is lacking. Most likely, the forest cover has been prohibiting shallow slope failure on the steep slopes with shallow soils in this zone in the past.

4.1.2. Central — Bukigai

No landslides were observed on the very steep slopes of the central Bukigai zone. The absence of landslides can be partly attributed to the soil types in this zone. The soils were designated as Acrisols and Ferralsols, physically stable soils without swell–shrink properties

Table 1
Soil physical parameters for soil type associations of the different zones used in the LAPSUS-LS model (Eqs. (1)–(5))

Zone	C [–]±SD	ϕ [rad]±SD	ρ_s [g/cm^3]±SD	T [m^2 day^{-1}]
Nusu/Bukalasi	0.15±0.04	0.7±0.07	1.6±0.04	15
Bukigai	0.47±0.07	0.5±0.10	1.5±0.07	17
Bududa/Bushika	0.35±0.09	0.4±0.07	1.6±0.06	17

wherein landslides rarely occur (Breugelmans, 2003). Still, these soils are very vulnerable to water erosion and low fertility does not favor agriculture and human settlement (Driessen and Dudal, 1991). Together with a lack of groundwater, this causes a low population density in Bukigai compared to the other regions where population pressure is an important factor for landsliding.

4.1.3. West — Bududa/Bushika

In the Bududa/Bushika zone, deep rotational slumps occur in Nitisols, soils with slight swell–shrink properties. All landslide scarps in this zone show a similar profile of at least two buried soils, created by an alternation of stable pedogenesis phases and unstable phases of regressive erosion. The superposition of a soil horizon with a silty clay texture on top of a coarser, sandy silt loam horizon of an older soil creates a pore discontinuity that hinders vertical drainage. As a result positive pore water pressures can develop, creating conditions which overcome the sliding inertia. In addition, the gentle slopes of the Bududa/Bushika zone have the highest population density, which might imply an increased human impact on hillslope stability (Knapen et al., 2006). Excavation of slopes and the concentration of runoff water through linear landscape elements (e.g. parcel boundaries, footpaths) are the main malefactors. Since the bedding planes of the substrata are parallel to the overall slope, excavation is particularly destabilizing here. The succession of different buried stone layers and soils suggests the presence of other discontinuities in the profile that can be responsible for the formation of deeper shear planes (Breugelmans, 2003).

4.2. LAPSUS-LS landslide hazard

The relative hazard for shallow landsliding (Q_{cr}; Eq. (1)) was calculated for the study catchment by the LAPSUS-LS model using the 10×10 m DEM and soil physical parameters from Table 1. Being relative measures of landslide susceptibility rather than physically

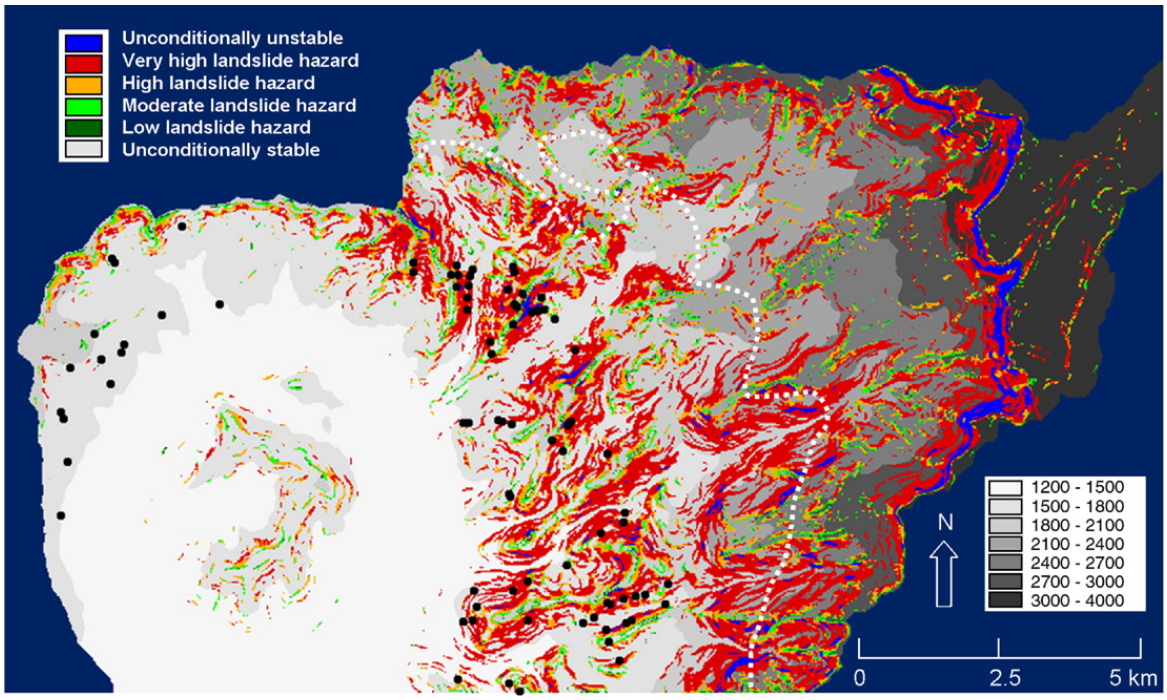

Fig. 2. Overlay of classified landslide hazards (Q_{cr}, legend top left) calculated with LAPSUS-LS and the classified DEM (legend down right) for the study area. Observed landslides from the 2002 survey are indicated as black dots.

Table 2
Overview and statistical comparison for LAPSUS-LS critical rainfall values (landslide hazard or Q_{cr} from Eq. (1) and DEM derived topographic attributes for Nusu/Bukalasi landslide sites (2002 survey, $n=66$) and the whole watershed

	Extent	Min	Max	Mean
Critical rainfall	Watershed[1]	$2 \cdot 10^{-5}$	0.779	0.049
Q_{cr} [m day^{-1}]	Landslides	0.005	0.141	0.040
Contributing area (multiple flow)	Watershed	1	1,472,369	1152.38
[#cells]	Landslides	3.48	138.81	20.02
Contributing area (steepest descent)	Watershed	1	1,476,273	1126.56
[#cells]	Landslides	1	244	23.5
Aspect	Watershed	−1 (flat)	360	211.71
[° from north]	Landslides	59.0422	357.11	219.65
Altitude	Watershed	1229.3	3848.30	2032.69
[m]	Landslides	1499.02	2019.51	1713.32
Slope	Watershed	0	80.01	20.37
[°]	Landslides	22.59	45.11	33.54
Profile curvature	Watershed	−21.91	45.66	0.015
[1/100 z units]	Landslides	−0.88	0.73	0.008
Plan curvature	Watershed	−48.64	28.19	0.015
[1/100 z units]	Landslides	−1.92	1.86	−0.08

[1]For Q_{cr} values, the landslide sites are only compared with positions having a valid Q_{cr} value (i.e. not unconditionally stable or unstable according to Eqs. (3) and (4) respectively).

interpretable absolute numbers, the Q_{cr} values were classified in six classes:

1) Unconditionally unstable according to Eq. (4).
2) Very high landslide hazard: $0.0 < Q_{cr} \leq 0.05$ m day^{-1}
3) High landslide hazard: $0.05 < Q_{cr} \leq 0.1$ m day^{-1}
4) Moderate landslide hazard: $0.1 < Q_{cr} \leq 0.2$ m day^{-1}
5) Low landslide hazard: $0.2 < Q_{cr}$ m day^{-1}
6) Unconditionally stable according to Eq. (3).

In Fig. 2, an overlay of classified landslide hazards from the LAPSUS-LS model with the DEM is depicted, as well as 81 mapped landslides from the 2002 survey. A first visual interpretation shows that in general, slopes in the eastern part (Nusu/Bukalasi) of the study area are relatively much more prone to landsliding than the central (Bukigai) and western (Bududa/Bushika) parts. Furthermore, the model only 'captures' the landslides in the east: all 66 shallow landslides mapped in the eastern zone are assigned a landslide hazard, whereas only 1 out of 15 deep rotational landslides in the western zone is getting a valid Q_{cr} value (i.e. not unconditionally stable or unstable; Eqs. (3) and (4)) in the simulation. This observation is in accordance with the underlying physical principles of the model: only shallow, topographically controlled landslides can be modeled using the equations derived (Montgomery and Dietrich, 1994; Borga et al., 2002; Claessens et al., in press). In the western zone, LAPSUS-LS assigns a shallow landslide hazard to positions upslope of the sites where the deep rotational landslides occur. Indeed the model is not suitable to predict positions of deep rotational slides, as mechanisms other than topographical concentration of subsurface flow, are important in activating the deeper shear planes (e.g. bypass flow through linear landscape elements or swell–shrink soil cracks). Consequently, only the 66 shallow landslides mapped in the Nusu/Bukalasi zone will be retained in further analysis. In the central zone, no landslides were observed and the model only delineates a few spots with a very low landslide hazard.

Although critical rainfall values calculated with LAPSUS-LS can only be interpreted as relative landslide hazard indexes, it is clear from the classified landslide hazard map (Fig. 2) that slopes of the Manjiya study area in general are very prone to landsliding. Topographic attributes and soil physical characteristics of the area make the slopes in the landscape inherently unstable. In addition, human interference enhances the landslide problem as population pressure forces people to occupy steep and unsafe slopes. Activities like terracing, undercutting of unstable slopes and the concentration of runoff water and infiltration in concavities by footpaths, roads, plot boundaries and other linear elements are major triggering factors for landsliding (Knapen et al., 2006).

4.3. Digital terrain analysis

In order to get an insight into the causal factors for the recent shallow landslides in the eastern part of the study area, descriptive statistics and histograms for explanatory topographic attributes from a digital terrain analysis (see Section 3.3) were constructed. In Table 2 a comparison of statistical data is made for the topographic attributes derived from the DEM, also including the relative landslide hazard calculated with LAPSUS-LS, between recent landslide sites from the Nusu/Bukalasi zone and the whole study catchment (Fig. 2). Fig. 3 gives an overview of the distribution as (cumulative) histograms of those attributes for the shallow landslide positions solely. From both Table 2 and Fig. 3 it is apparent that the majority of landslide sites have a relative landslide hazard (critical rainfall) of about 0.03–0.05 m day^{-1}. The LAPSUS-LS model is capable of classifying the Nusu/Bukalasi landslides from the 2002 survey in a rather narrow landslide hazard class. This can be used in the modelling of landslide scenarios (see

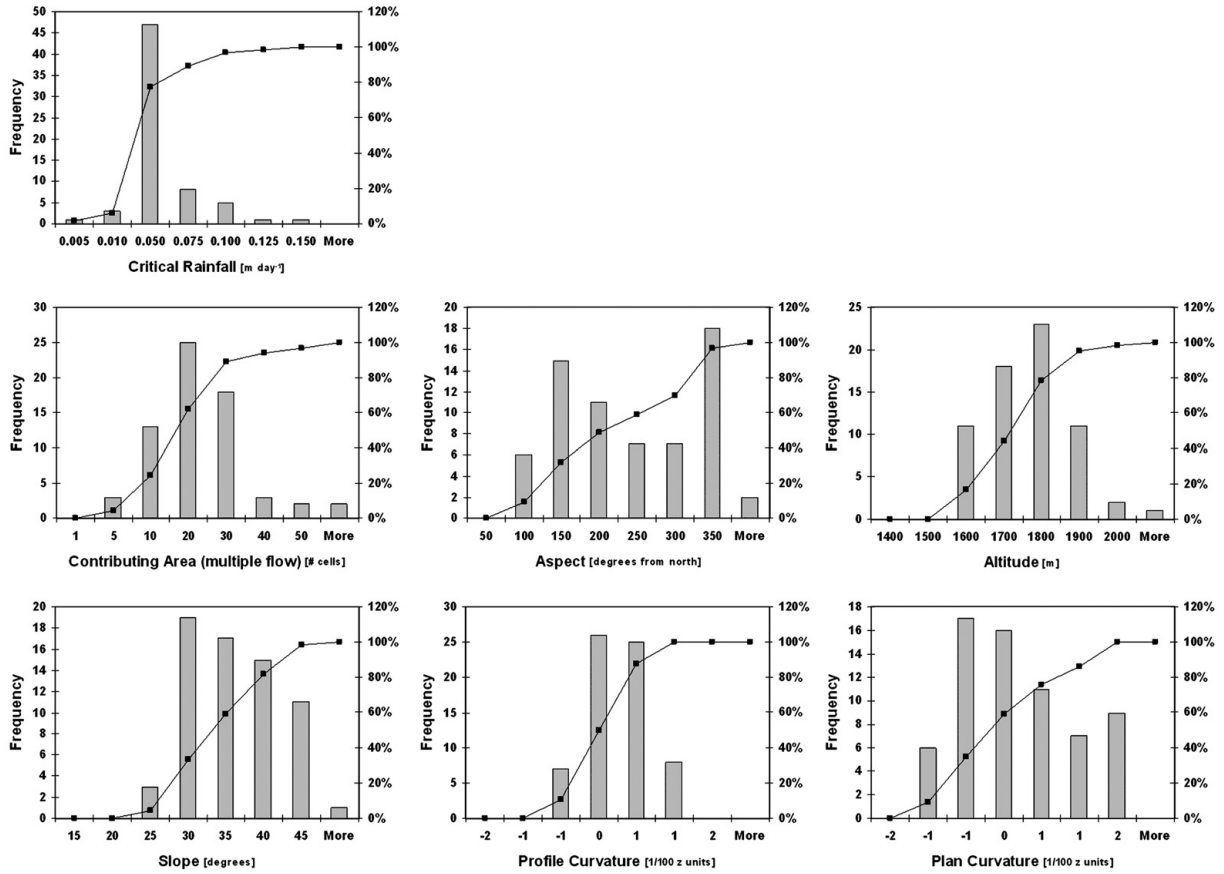

Fig. 3. Histograms and cumulative histograms for LAPSUS-LS critical rainfall values (Q_{cr}, landslide hazards) and topographic attributes derived from the 10 × 10 m DEM for the 2002 Nusu/Bukalasi landslide sites (n = 66).

next section). It must be stressed again that the values of critical rainfall (although in m day^{-1}) cannot be interpreted as 'real' rainfall values but must rather be seen as relative indexes of shallow landslide hazard (Borga et al., 2002; Claessens et al., 2006a).

Regarding contributing area, calculated with both steepest descent and multiple flow routing algorithms (Table 2), most landslide sites have values between 20 and 40 grid cells of 10×10 m, implying a typical upslope catchment area of 2000–4000 m^2. Regarding aspect, most landslide sites in Nusu/Bukalasi are oriented north and south, as can be seen from the histogram in Fig. 3. This does not confirm the more general northeast aspect, which is the dominant rainfall direction, for landslides in the whole study area as found by Knapen et al. (2006). Calculating aspects on a cell to cell basis from the DEM, rather than using the more overall field characteristics as observed by Knapen et al. (2006), can possibly explain this different dominant aspect. Most landslides occur in an altitude range of 1600–1900 m, which apparently coincides with the altitude zone receiving the required contributing area from upslope to trigger the landslides. Slope angles of landslide positions are in the range of 30–40°, which can be linked with the internal friction angle for soils in this area (0.7 rad=40° for Nusu/Bukalasi, Table 1). Profile curvature values are only slightly tending towards positive, indicating that soil surfaces are generally concave at landslide positions. Most landslides seem to occur on the transition between steep upslope positions, where slope is increasing downhill, towards more concave positions, where slope is decreasing and water tends to accumulate. Plan curvature values are slightly negative, pointing to converging flows typical for local valleys or channels. Also here, landslides seem to occur at the transition between diverging and converging flow, again positions where water is expected to accumulate and trigger shallow landslides. In general, the topographic attributes determining positions of slope failure point to concentration of (sub)surface flow as the main hydrological triggering mechanism for shallow landslides in the study area. This also explains why on the steepest slopes less landslides occur, as these ridgetop positions generally do not have the required contributing area for slope failure by water concentration.

4.4. Soil redistribution and sediment yield

The 2002 field survey showed that the 81 mapped landslides together displaced ca. 10 million m^3 of slope material. Erosion and sedimentation by landslides caused fatalities, serious property damage and significant geomorphic effects in the recent past. Over recent decades, at least 29 landslides have dammed rivers in Manjiya for some time and river patterns as well as drainage areas have been changed by them. Fast flows of landslide debris temporarily dammed water channels and damaged infrastructure when the dams broke. In 1997 at least 48 people were killed, crops and dwellings of 885 families were destroyed, 5600 people became homeless, arable land was reduced, water supplies were polluted and finally Manjiya was hit by food-shortage (Ministry of Water, Lands and Environment Uganda, 2003). Although landslides from the beginning of the 20th century could be located during the 2002 field survey, most of the mapped landslides are relatively young: 70% occurred since 1997 and the majority (52%) during the heavy rains of 1997 to 1999. Furthermore, the shallow landslides on the eastern slopes might already be recultivated after some years, and the material displaced by the mapped landslides is definitely an underestimation of the longer-term soil loss due to mass movement in the study area.

To simulate the possible future effects of landslides on soil redistribution quantities and catchment sediment yield, the LAPSUS-LS model is used. We simulated a scenario representative of the conditions having caused the 66 recent shallow landslides from the Nusu/Bukalasi zone mapped in the field survey. The mean landslide hazard index for the landslides (i.e. the average critical rainfall value, being 0.040 m day^{-1}) is used as a threshold value for landslide initiation. In this scenario, all sites having a critical rainfall value lower than 0.040 m day^{-1} (meaning a higher landslide hazard than the mean hazard for the mapped landslides) are failing and enter the soil redistribution and sediment yield algorithms of the LAPSUS-LS model (Eqs. (5)–(8) and Section 3.2.3). By modelling the spatial pattern of landslide soil redistribution and the interaction with the channel network, buffering of the depositional response by temporary storage of landslide material on footslopes is taken into account. If the depositional pathway does not cross a transporting channel, the landslide material is not delivered to the outlet but remains on the slope and hence is excluded from the sediment yield. The delivery ratio is also determined by using this method (and does not need to be estimated): deposition that occurs out of reach of a channel capable of transporting the material is not added to the sediment yield.

The results for this scenario, according to the LAPSUS-LS model, are a total estimated volume of 44,099,994 m^3 of soil material displaced by shallow landslides in the 13,360 ha catchment. The fraction of this ending up in the stream network and contributing to

the catchment sediment yield is estimated by the model to amount to 23,739,514 m^3. This scenario indicates that the total volume of eroded material and sediment deposited caused by shallow landslides could be four times higher than the total volume observed in the 2002 field survey (ca. 10 million m^3 soil material displaced, for both shallow and deep landslides). In addition, more than half of this soil material can reach the stream network, possibly damming rivers and causing major damage to infrastructure or siltation and pollution of streams. It should be noted however that the part of the study area within Mount Elgon National Park (Fig. 1) has been assigned the same LAPSUS-LS parameter setting as the eastern Nusu/Bukalasi zone in general, having a lumped zero value for root cohesion (see Section 3.3). Landslide hazard and the associated soil redistribution following the modeled scenario are surely overestimated for this area where the tropical montane forest vegetation in the national park contributes significantly to increased soil strength by root reinforcement. It however gives an indication of what the consequences of further deforestation beyond the park's boundaries could be. On the other hand, only shallow landslides are simulated in the model scenario. Deep rotational landslides, which occur mainly in the western part of the study area, are not taken into account for but do contribute to the total sediment yield, which is in this way underestimated in the model simulation.

5. Conclusions

Using an existing data set of 81 mapped landslides in the Manjiya study area on the slopes of Mount Elgon in Uganda (Knapen et al., 2006), the LAPSUS-LS landslide model (Claessens et al., in press) and digital terrain analysis were applied. The methodology was used to delineate landslide positions and hazards, analyze causal factors for landslides and simulate future landslide scenarios and their geomorphic effects on the densely populated catchment. As expected from the original setup and underlying physical principles of the LAPSUS-LS model, only shallow landslides occurring mainly in the eastern part of the study area could be predicted and classified correctly. The deeper rotational landslides in the western part could not be 'captured' by the model as only shallow, topographically controlled landslides can be simulated using the equations derived (Montgomery and Dietrich, 1994; Borga et al., 2002; Claessens et al., in press). By statistically analyzing the topographic attributes associated with the 66 shallow landslide sites in the eastern Nusu/Bukalasi zone, most of the causal factors determined in the previous study (Knapen et al., 2006), were confirmed. In general, shallow landslides occur at a relatively large distance from the water divide, on the transition between steep concave and more gentle convex slope positions. This trend points to concentration of (sub)surface flow as the main, topographically controlled, hydrological triggering mechanism. The LAPSUS-LS model is capable of grouping the 66 landslide positions into a narrow relative landslide hazard class of critical rainfall values ranging from 0.03 to 0.05 m day^{-1}. This specific landslide hazard index was used as a threshold to simulate a future landslide scenario, also using the LAPSUS-LS soil redistribution algorithms. According to the model, the volume of soil material displaced could be four times higher than that observed in the 2002 field survey (44,099,994 m^3). In addition, more than half of this volume is predicted to end up in the stream network and so contribute to the catchment sediment yield. This soil material can cause damming of rivers causing major damage to property or siltation and pollution of streams.

A landslide hazard map for the study area was constructed by overlying the classified critical rainfall values calculated with LAPSUS-LS with the DEM (Fig. 2). From this map it is apparent that slopes of the Manjiya catchment can be regarded as inherently unstable, and that landslides will remain a major problem. Most of the causes for mass movement are inherent characteristics of the study area, merely dictated by soil physical properties and topography. Therefore solutions for the landslide problem are difficult to find. As population pressure increases, not only the stability of the slopes will be reduced, but people will also be forced to cultivate even more unstable slopes. As pointed out by Knapen et al. (2006), the instability could partly be reduced by tempering the human impact (e.g. by avoiding excavation or terracing of slopes and construction of structures concentrating water to vulnerable zones). In addition, reforestation with deep-rooted trees could effectively reduce the shallow landslide hazard on certain landscape positions. Still, these measures can never completely prevent the occurrence of landslides and a long-term solution for the problem can only be found in offering alternatives to inhabitants or encourage family planning to make fast population growth take a turn.

Acknowledgements

Funding for the initial fieldwork was provided by the Belgian Technical Cooperation (BTC), the World Conservation Union (Mount Elgon Conservation

Project) and the fund for Scientific Research Flanders. Farmers and officers of Manjiya and the Department of Geology at Makerere University (Uganda) provided information and logistic support. Financial support from the Katholieke Universiteit Leuven (Belgium) and the USAID Soil Management Collaborative Research Support Program (SM-CRSP) is gratefully acknowledged. The authors also thank Nel Caine, Wilson Mwaniki Ngecu, Takashi Oguchi and Gerard Heuvelink for their valuable comments which improved the paper.

References

Blocken, B., Poesen, J., Carmeliet, J., 2006. Impact of wind on the spatial distribution of rain over micro-scale topography: numerical modelling and experimental verification. Hydrological Processes 20, 345–368.

Borga, M., Dalla Fontana, G., Gregoretti, C., Marchi, L., 2002. Assessment of shallow landsliding by using a physically based model of hillslope stability. Hydrological Processes 16, 2833–2851.

Breugelmans, W., 2003. The influence of soil, land use and deforestation on the occurrence of landslides in Mount Elgon area, Eastern Uganda. Unpublished MSc thesis, Catholic University Leuven, Belgium.

Burton, A., Bathurst, J.C., 1998. Physically based modelling of shallow landslide sediment yield at a catchment scale. Environmental Geology 35, 89–99.

Christiansson, C., Westerberg, L.O., 1999. Highlands in East Africa: unstable slopes, unstable environments. Ambio 18, 419–429.

Claessens, L., Heuvelink, G.B.M., Schoorl, J.M., Veldkamp, A., 2005. DEM resolution effects on shallow landslide hazard and soil redistribution modelling. Earth Surface Processes and Landforms 30, 461–477.

Claessens, L., Lowe, D.J., Hayward, B.W., Schaap, B.F., Schoorl, J.M., Veldkamp, A., 2006a. Reconstructing high-magnitude/low-frequency landslide events based on soil redistribution modelling and a Late-Holocene sediment record from New Zealand. Geomorphology 74, 29–49.

Claessens, L., Verburg, P.H., Schoorl, J.M., Veldkamp, A., 2006b. Contribution of topographically based landslide hazard modelling to the analysis of the spatial distribution and ecology of kauri (*Agathis australis*). Landscape Ecology 21, 63–76.

Claessens, L., Schoorl, J.M., Veldkamp, A., in press. Modelling the location of shallow landslides and their effects on landscape dynamics in large watersheds: an application for Northern New Zealand. Geomorphology. doi:10.1016/j.geomorph.2006.06.039.

Davies, K.A., 1957. The building of Mount Elgon (East Africa). The Geological Survey of Uganda, Entebbe, Uganda.

Davies, T.C., 1996. Landslide research in Kenya. Journal of African Earth Sciences 23, 41–49.

Deckers, J.A., Nachtergaele, F.O., Spaargaren, O.C., 1998. World Reference Base for Soil Resources. Acco, Leuven/Amersfoort. 165 pp.

Driessen, P.M., Dudal, R., 1991. The Major Soils of the World. Department of Soil Science and Geology. Wageningen Agricultural University, The Netherlands.

Fairfield, J., Leymarie, P., 1991. Drainage networks from grid digital elevation models. Water Resources Research 27, 709–717.

Glade, T., Crozier, G.M., 2004. The nature of landslide hazard impact. In: Glade, T., Anderson, M.G., Crozier, G.M. (Eds.), Landslide Hazard and Risk. Wiley, Chichester, pp. 43–74.

Hamilton, A.C., 1984. Deforestation in Uganda. Oxford University Press, Nairobi, Kenya.

Hutchinson, M.F., 1989. A new procedure for gridding elevation and stream line data with automatic removal of spurious pits. Journal of Hydrology 106, 211–232.

Knapen, A., 2003. Spatial and temporal analysis of landslides in Manjiya County, Mount Elgon area, eastern Uganda. Unpublished MSc thesis, Catholic University Leuven, Belgium.

Knapen, A., Kitutu, M.G., Poesen, J., Breugelmans, W., Deckers, J., Muwanga, A., 2006. Landslides in a densely populated county at the footslopes of Mount Elgon (Uganda): characteristics and causal factors. Geomorphology 73, 149–165.

Lands and Surveys Department Uganda, 1967. Topographic Map Series 1:50,000. Sheet Manjiya County. Lands and Surveys Department, Kampala, Uganda.

Martin, Y., Rood, K., Schwab, J.W., Church, M., 2002. Sediment transfer by shallow landsliding in the Queen Charlotte Islands, British Columbia. Canadian Journal of Earth Sciences 39, 189–205.

Ministry of Water, Lands and Environment Uganda, 2003. Briefing Document on Climate Change and Its Impacts. Kampala, Uganda.

Moeyersons, J., 1989. A possible causal relationship between creep and sliding on Rwaza hill, Southern Rwanda. Earth Surface Processes and Landforms 14, 597–614.

Moeyersons, J., 2003. The topographic thresholds of hillslope incisions in southwestern Rwanda. Catena 50, 381–400.

Montgomery, D.R., Dietrich, W.E., 1994. A physically-based model for the topographic control on shallow landsliding. Water Resources Research 30, 1153–1171.

Montgomery, D.R., Schmidt, K.M., Greenberg, H.M., Dietrich, W.E., 2000. Forest clearing and regional landsliding. Geology 28, 311–314.

Moore, I.D., Grayson, R.B., Ladson, A.R., 1991. Digital terrain modeling — a review of hydrological, geomorphological, and biological applications. Hydrological Processes 5, 3–30.

Moore, I.D., Norton, T.W., Williams, J.E., 1993. Modelling environmental heterogeneity in forested landscapes. Journal of Hydrology 150, 717–747.

Muwanga, A., Schuman, A., Biryabarema, M., 2001. Landslides in Uganda — documentation of a natural hazard. Documenta Naturae 136, 111–115.

National Environment Management Authority, 2001. State of the environment report for Uganda 2000/2001. National Environment Authority, Kampala, Uganda.

Ngecu, W.M., Ichangi, D.W., 1998. The environmental impact of landslides on the population living on the eastern footslopes of the Aberdare Ranges in Kenya: a case study of Maringa village. Environmental Geology 38, 259–264.

Ngecu, W.M., Mathu, E.M., 1999. The El Niño-triggered landslides and their socioeconomic impact on Kenya. Environmental Geology 38, 277–284.

Nyssen, J., Moeyersons, J., Poesen, J., Deckers, J., Mitiku, H., 2002. The environmental significance of the remobilization of ancient mass movements in the Atbara–Tekeze headwaters near Hagere Selam, Tigray, Northern Ethiopia. Geomorphology 49, 303–322.

O'Callaghan, J.F., Mark, D.M., 1984. The extraction of drainage networks from digital elevation data. Computer Vision, Graphics, and Image Processing 28, 323–344.

Pack, R.T., T, D.G., Goodwin, C.N., 2001. Assessing terrain stability in a GIS using SINMAP, 15th annual GIS conference, Vancouver, British Columbia.

Quinn, P., Beven, K., Chevallier, P., Planchon, O., 1991. The prediction of hillslope flow paths for distributed hydrological

modeling using digital terrain models. Hydrological Processes 5, 59–79.

Reedman, J.H., 1973. Potash ultra-fenites at the Butiriku carbonatite complex in southeast Uganda. Annual Report, vol. 17. Research Institute for African Geology, University of Leeds, pp. 78–81.

Schoorl, J.M., Sonneveld, M.P.W., Veldkamp, A., 2000. Three-dimensional landscape process modelling: the effect of DEM resolution. Earth Surface Processes and Landforms 25, 1025–1034.

Uganda Bureau of Statistics, 2004. The 2002 Uganda Population and Housing Census. Entebbe, Uganda.

Vandre, B.C., 1985. Rudd Creek debris flow. In: Bowles, D.S. (Ed.), Delineation of Landslide, Flash Flood, and Debris Flow Hazards in Utah. Utah Water Research Laboratory, Utah State University, Logan, Utah, pp. 117–131.

Westerberg, L.O., Christiansson, C., 1998. Landslides in East African Highlands. Slope instability and its interrelations with landscape characteristics and land use. Advances in GeoEcology 31, 317–325.

Wilson, J.P., Gallant, J.C., 2000. Terrain Analysis: Principles and Applications. John Wiley and Sons, Chichester.

Zevenbergen, L.W., Thorne, C.R., 1987. Quantitative analysis of land surface topography. Earth Surface Processes and Landforms 12, 47–56.